EXPERIMENTAL INVESTIGATION OF AIR ENTRAINMENT AT A REACTOR CONTAINMENT SUMP DUE TO BREAK AND DRAIN FLOWS

DONALD C. COOK NUCLEAR POWER STATION

by

Mahadevan Padmanabhan
John F. Noreika
Carl R. Janik

Research Sponsored by
American Electric Power Service Corporation

George E. Hecker, Director

ALDEN RESEARCH LABORATORY
WORCESTER POLYTECHNIC INSTITUTE
HOLDEN, MASSACHUSETTS

December 1979

ABSTRACT

American Electric Power Service Corporation (AEPSC) authorized the Alden Research Laboratory (ARL) of Worcester Polytechnic Institute (WPI) to conduct extensive hydraulic model testing of the Reactor Containment Sump of the Donald C. Cook Nuclear Power Plant, Units 1 and 2. The model studies were conducted in two phases.

A separate report of the first phase of the model studies to investigate vortexing, swirl, and inlet losses was submitted earlier (ARL Report No. 108-78/M178PF, September 1978). The main purpose of the second phase of the model studies reported herein was to verify that the reactor containment sump would perform satisfactorily without the development of objectionable air-entrainment due to break flow and drain flow impingement through the water surface near the sump. Such possible air-entrainment could affect the operation of the pumps in the Emergency Core Cooling System (ECCS) during the recirculation mode.

A model based on Froude similarity was designed and constructed to a scale of 1:2.5 to include the sump and the surrounding area of the containment building with all the structures that could influence the approach flow. Revisions to the sump configuration based on the vortexing and swirl studies conducted earlier were incorporated in the model. Possible scale effects of modeling air entrainment due to jet impingement were considered and a suitable test procedure was developed involving testing at higher than Froude scaled jet velocities and suction pipe velocities. Tests were conducted incorporating various possible flow and pump combinations, along with possible break and drain flows near the sump area, including different possible screen blockage.

It was determined that redirecting of ice condenser drain pipes away from the sump area was desirable to reduce excessive air entrainment within the sump and to eliminate air bubbles being carried to the suction pipes under certain screen blockage conditions. Break flow impingement tests did not indicate any significant air-entrainment and, hence, no modifications in the sump geometry itself was felt necessary.

TABLE OF CONTENTS

INTRODUCTION

The reactor containment buildings of the Donald C. Cook Nuclear Power Station, Units 1 and 2, are provided with emergency core cooling systems (ECCS) designed to cool the shutdown reactor cores and the containments in the event of a loss of coolant accident (LOCA). The ECCS injects water to maintain core cooling and, initially, the water for this is drawn from the refueling water storage tank (RWST). When the water level in this tank is depleted to a predetermined level, the ECCS is switched from injection to recirculation mode. At this point, water is drawn from the containment recirculation sump containing water drained from the break, water from the ice condenser meltdown, and water from the containment spray system. The approach flow to the sump is affected by the equipments and appurtenant structures in the flow path. The water level, the pump discharges, and the water temperature could vary over a wide range during the recirculation mode, which lasts for an extended period of time to provide sufficient heat removal. The break flow and drain flow vary with time and they impinge on the water surface as a high velocity jet. It is very important that no adverse flow conditions caused by break and ice drain flow jets exist within the sump or the suction pipes that could affect performance of the pumps.

The Alden Research Laboratory (ARL) was authorized by American Electric Power Service Corporation (AEPSC) to construct and test a model of the Donald C. Cook Nuclear Power Station containment recirculation sump with the object of investigating free surface vortex formation, swirl, inlet losses, air entrainment due to impingement, or any other undesirable flow conditions that could adversely affect the performance of the Residual Heat Removal (RHR) and Containment Spray Pumps (CTS), and Safety Injection (SI) Pumps of the Emergency Core Cooling Water System (ECCS) in the recirculation mode. Operating conditions involving a wide range of various possible approach flow distributions, water depths, water temperatures, screen blockage effects, and pump operating combinations were to be tested in the model. If potentially undesirable flow condi-

tions occurred, modifications in the sump configuration were to be developed. The first phase of the model study was the investigation of air entrainment due to vortexing, suction of entrapped air, swirl in the suction pipes, and the inlet losses at the sump and the details of this phase were included in a separate ARL report (1).

This report presents the findings of the second phase of the study involving break and drain flow impingement and includes a description of the prototype and model, and summarizes conditions investigated, similitude considerations, test procedures, instrumentation, interpretation of results, and conclusions.

PROTOTYPE DESCRIPTION

Reactor Building

The reactor building is circular in plan with two concentric outer walls; namely, the crane wall and the containment wall, with inner radii of 41.5 ft and 57.5 ft, respectively. The steam generators, reactor coolant pumps, containment cleanup filter units, and the connected accessories are all located in the portion between the reactor chamber and the crane wall, as seen in Figure 1. The annular portion between the crane and containment walls accommodated the various pipes, valves, air ducts, and cables for various operating systems, such as blowdown, cooling water, ventilation, and liquid waste recycling.

The Containment Recirculation Sump

The Containment Recirculation sump is located close to the crane wall between the steam generator number 2 and reactor coolant pump number 2 (extending from bearing 120 to 150 degrees approximately), as marked in Figure 1. The sump is more or less rectangular in plan, about 18 ft long and 10.5 ft wide, with the crane wall dividing it into two portions.

Recirculation flow enters the upstream portion through stainless steel gratings and screens provided at the entrance, continues down and under the crane wall, and finally enters the suction pipes. Figure 2 shows the sump details and illustrates that the upstream portion would have a free surface while the downstream portion would be under pressure. The top slab of the downstream portion of the sump is provided with a single air vent pipe running upward through the crane wall. The sump floor is at EL 591 ft 1 inch, whereas the building floor is at EL 598 ft 9-3/8 inches. The average approach velocity upstream of the grating would be about 0.34 fps at the minimum submergence (EL 602 ft 10 inches).

The two outlet pipes are 18 inches in diameter (Sch. 40), and are provided with bellmouth entrances and 24 inch diameter guard pipes. The suction pipes run downward at an inclination of 13°34' to horizontal, as shown in Figure 2. The center of the pipe entrance is at EL 595 ft 6 inches, and each pipe is connected to a valve at EL 589 ft 9 inches.

As indicated in Figure 1, a lower sump, rectangular in plan (about 2 ft 4 inches by 4 ft, 10 inches), and 7 ft 8-3/8 inches deep, is provided adjacent to the main containment sump to allow for proper drainage in normal conditions. This sump is connected to the main containment sump by an 8 inch diameter pipe.

Break Flow Locations

The possible break flow locations in the sump vicinity (provided by AEPSC) are located in the cross-over, high pressure pipe connecting the reactor coolant pump and steam generator, as indicated in Figure 3. There are six break locations in this loop with two additional break locations, one each in the 3 inch and 2 inch pipes attached to the loop at the bottom straight portion. The hot leg joining the steam generator to the reactor has one break location. The six breaks in the cross-over loop and the one break in the hot leg are all circumferential type breaks. The 3 inch and 2 inch

pipe breaks will cause circular jets issuing vertically up or down. The break area resulting from the axial displacement for the breaks in the cross-over loop and hot leg is approximately 25.0 square inches. Table 1 indicates the rate of break flow following a LOCA.

The four ice condenser drain flow locations close to the sump (four locations) are indicated in Figure 4. The drains are 12 inches in diameter and terminate horizontally at about 36 ft from the building floor. The drains may not be flowing full for most of the time. The drain flowrate following LOCA is given by the curve shown in Figure 5.

The break flow and drain flow locations will be identified hereafter in this report by the numbers given in Figures 3 and 4.

Operating Cases for Tests

The discharge and submergence conditions at the sump would change with the different operating sequences from the instant of a LOCA. The following system operations were considered important in investigating the hydraulic performance of the sump:

1. 9500 gpm through one suction pipe - This simulates the runout condition of one ECCS train upon complete failure of the other train.

2. 7700 gpm per suction pipe, both pipes operating - This simulates the runout condition of ECCS pumps with both trains operating.

3. 9500 gpm through one pipe and 3600 gpm through the other - Same as case 1 except that the containment spray pump from the other train is at runout flowrate.

Should a LOCA occur in any of the break locations described earlier, the ECCS pumps, which are aligned to the refueling water storage tank (RWST), would inject 350,000 gallons of borated water into the primary loop before the recirculation sump is completely used. One train of ECCS pumps would be switched to the recirculation sump when the water level in the RWST reaches a predetermined low level, the time for this being about 10 minutes after the start of ECCS.

It is not until the RWST reaches the lowest level that the second train of ECCS pumps would be switched to the recirculation sump. At this time, the entire 350,000 gallons would have been pumped into the sump via the primary loop.

A water level of 602 ft, 10 inches is the elevation at which the first ECCS train suction supply would be switched from the Refueling Water Storage Tank (RWST) to the containment recirculation sump. A water level of EL 606 ft will be the point at which the suction source of the second string of ECCS would be switched from the RWST to the containment recirculation sump.

The above levels are calculated by APESC assuming that the breaks in the primary system occur inside the biological boundary. This assumption results in the lowest possible containment levels since it postulates that approximately 128,000 gallons of fluid must spill within the biological barrier before any fluid spills into the recirculation sump cavity. This, of course, is conservative and the above water levels are used for model tests with drain flows but no break flows near the sump portion.

Jet impingement modeling with break flow near the sump is based on a break in the primary system occurring outside the biological boundary (if it were inside, it could have no effect on the sump). Therefore, the 128,000 gallons which was considered unavailable within the biological boundary is now available to supply additional fluid inventory outside the boundary. Since the containment water level outside the boundary will rise approximately 1 ft per additional 28,000 gallons of fluid (as per APESC), the total rise will be approximately 4.5 ft. The new water levels would then be 607 ft 4 inches for first ECCS switchover and 610 ft for second ECCS switchover.

Table 2 summarizes the system operations, each of which, for convenience, will be identified by the case number hereafter in this report. The water temperature of the breakflow, which would be collected in the sump, could be as high as 190°F. A containment pressure of up to 3.0 psig would be possible.

AIR ENTRAINMENT DUE TO JET IMPINGEMENT

High velocity jets impinging on a water surface are known to produce considerable air entrainment. If such a condition exists very close to the sump, the approach flow will draw with it a large number of air bubbles into the sump. For the particular sump configuration of the D.C. Cook plant, all bubbles which have rise velocities less than the downward velocity of the flow in the upstream portion of the sump are likely to be carried underneath the crane wall. The bubbles may get entrained in the main flow towards the suction pipes, and would be drawn into the pipes. If sufficient retention time is available, the bubbles could reach the top cover and get collected or escape through the venting system, depending on its effectiveness. Bubbles collected on the top cover may coalesce to form air pockets, and these air pockets could be drawn intermittently into the suction pipes as slugs, or could help form air-core vortices.

It is evident that even a low air concentration in the suction pipes, such as 5%, could lower the efficiency of the pump considerably (2). Further, air-water mixture flow could generate pressure fluctuations on the impeller. Hence, air entrainment is recognized as a potential adverse condition to be examined.

SIMILITUDE

The study of dynamically similar fluid motions forms the basis for the design of models and the interpretation of experimental data. The basic concept of dynamic similarity may be stated as the requirement that two systems with geometrically similar boundaries have geometrically similar flow patterns at corresponding instants of time (3). Thus, all individual forces acting on corresponding fluid elements of mass must have the same ratios in the two systems.

The condition required for complete similitude may be developed from Newton's second law of motion:

$$F_i = F_p + F_g + F_v + F_t \qquad (1)$$

where

F_i = inertia force, defined as mass, M, times the acceleration, a

F_p = pressure force connected with or resulting from the motion

F_g = gravitational force

F_v = viscous force

F_t = force due to surface tension

Additional forces may be relevant under special circumstances, such as fluid compression, magnetic or Coriolis forces, but these had no influence on this study and were, therefore, not considered in the following development.

Equation (1) can be made dimensionless by dividing all the terms by F_i. Two systems which are geometrically similar are dynamically similar if both satisfy the dimensionless form of the equation of motion, Equation (1). We may write each of the forces on the right side of Equation (1) as:

F_p = net pressure x area = $\alpha_1 \Delta p L^2$

F_g = specific weight x volume = $\alpha_2 \gamma L^3$

F_v = shear stress x area = $\alpha_3 \mu \Delta u/\Delta y$ x area = $\alpha_3 \mu u L$

F_t = surface tension x length = $\alpha_4 \sigma L$

F_i = density x volume x acceleration = $\alpha_5 \rho L^3 u^2/L = \alpha_5 \rho u^2 L^2$

where

α_1, α_2, etc. = proportionality factors

L = representative linear dimension

Δp = net pressure

γ = specific weight

μ = dynamic viscosity

σ = surface tension

ρ = density

u = representative velocity

Substituting the above terms in Equation (1) and making it dimensionless by dividing the inertial force, we obtain

$$\frac{\alpha_1}{\alpha_5} E^{-2} + \frac{\alpha_2}{\alpha_5} F^{-2} + \frac{\alpha_3}{\alpha_5} R^{-1} + \frac{\alpha_4}{\alpha_5} W^{-2} = 1 \qquad (2)$$

where

$$E = \frac{u}{\sqrt{\Delta p/\rho}} = \text{Euler number} \propto \frac{\text{Inertia Force}}{\text{Pressure Force}}$$

$$F = \frac{u}{\sqrt{gL}} = \text{Froude number} \propto \frac{\text{Inertia Force}}{\text{Pressure Force}}$$

$$R = \frac{u\,L}{\mu/\rho} = \text{Reynolds number} \propto \frac{\text{Inertia Force}}{\text{Viscous Force}}$$

$$W = \frac{u}{\sqrt{\sigma/\rho L}} = \text{Weber number} \propto \frac{\text{Inertia Force}}{\text{Surface Tension Force}}$$

Since the proportionality factors, α, are the same in model and prototype, complete dynamic similarity is achieved if all the dimensionless groups, E, F, R, and W, have the same values in model and prototype. In practice, this is difficult to achieve. For example, to have the values of F and R the same requires either a 1:1 "model" or a fluid of very low kinematic viscosity in the reduced scale model. Hence, the accepted approach is to select the predominant force and design the model according to the appropriate dimensionless group. The influence of other forces would be secondary and are called scale effects (3). Special testing procedures may be established to determine or to account for scale effects approximately but usually conservatively.

Froude Scaling

Models involving a free surface are constructed and operated using Froude similarity since the flow process is controlled by gravity and inertia forces. The Froude number, representing the ratio of inertia to gravitational force,

$$F = u/\sqrt{gs} \qquad (3)$$

where

u = average velocity in the pipe
g = gravitational acceleration
s = submergence

was, therefore, made equal in model and prototype

$$F_r = F_m/F_p = 1 \qquad (4)$$

where m, p, and r denote model, prototype, and ratio between model and prototype, respectively.

In modeling of an intake sump to study the formation of vortices, it is important to select a reasonably large geometric scale to achieve large Reynolds numbers and to reproduce the curved flow pattern in the vicinity of the intake (4). A geometric scale of $L_r = L_m/L_p = 1/2.5$ was chosen for the model, where L refers to length. At higher Reynolds number, an asymptotic behavior of energy loss coefficients with Reynolds number is usually observed in similar flows. Hence, with $F_r = 1$, the basic Froudian scaling criterion, the Euler numbers, E, will be equal in model and prototype. This implies that flow patterns and loss coefficients are equal in model and prototype. From Equation (4), using $s_r = L_r$, the velocity, discharge, and time scales were:

$$u_r = L_r^{0.5} \tag{5}$$

$$Q_r = L_r^2 \, u_r = L_r^{2.5} \tag{6}$$

$$t_r = L_r^{0.5} \tag{7}$$

Similarity of Air-Entrainment Due to Jet Impingement

A. Dimensional Analysis

The major parameters influencing the rate of aeration of a rectangular jet impinging on a pool of water are (5):

a. The depth of fall (H)
b. The jet velocity at impact (u_j)
c. Jet width b and thickness d
d. Minimum impact velocity to cause air entrainment, u'_j
e. The jet perimeter, p
f. Froude number F_j, Reynolds number R_j, and Weber number W_j of the jet

For large scale air-entrainment caused by high velocity jets of relatively large thickness, the effect of R_j and W_j are negligible (5). Hence, the relative air concentration (volumetric quality) β, is given by:

$$\beta = f\left(F_j, \frac{H}{d}, \frac{u_j}{u'_j}, \frac{p}{d}\right) \tag{8}$$

The minimum impact velocity for air-entrainment, u_j is about 3.6 fps (5), and is considered a constant independent of other jet parameters. Based on experimental data, reference (6) gives

$$\beta = K \left(\frac{b}{p}\right) \left(\frac{H}{d}\right)^{0.446} \left(1 - \frac{u_j}{u'_j}\right) \tag{9}$$

where K is a function of F_j, but more or less independent of F_j if F_j is greater than 10. Hence,

$$\beta_r = \frac{\beta_m}{\beta_p} = \left(\frac{b}{p}\right)_r \left(\frac{H}{d}\right)_r^{0.446} \left(1 - \frac{u_j}{u'_j}\right) \tag{10}$$

assuming F_j is greater than 10 for model and prototype.

If the break area is modeled to chosen geometric scale with an assumed break width and thickness and the break locations are also correctly modeled to the geometric scale, then b/p and H/d values are conceivably the same in model and prototype. However, in this study, only the break area and height, H, are known beforehand whereas the values of b, p, and d are assumed making sure that their influence on the problem of concern is not overlooked.

From Equation (10), if $(b/p)_r$ and $(H/d)_r$ are equal to unity, β_r will be equal to unity only if the jet impact velocity is made equal in the model and prototype, u'_j being a constant. However, this is possible only if the chosen model is large enough. Also, if the values of H, p, and d are too small, scale effects, such as due to the influence of surface tension, may result. In the present study, the scale of 1:2.5 is considered sufficient by large.

B. Bubble Rise Velocities

High velocity jets of water impinging on a stagnant water surface produce a swarm of bubbles, the interaction between the bubbles causing a reduced rise velocity compared to that for single bubbles (7). The entrained air could be in the form of bubbles of varying sizes. Within a wide range of downfall jet velocities, the corresponding bubble size ranges have been observed to differ very little (8). This means that the model and prototype are likely to have more or less the same range of bubble sizes, even when the jet velocities and heights of fall are modeled using the Froude law of similarity. The rise velocity of bubbles are dependent on their sizes and the air concentration, β (7), and hence the rise velocities are not simulated to Froude velocity scale when a model is operated on Froude law. Air-entrainment measurements in a model operated on Froude law do not predict the air concentrations in the real situation, as evident from Equation (10). In fact, the prototype is likely to have higher air concentrations due to higher jet velocities.

As the bubble rise velocities are higher with lower air concentrations for same bubble size ranges, the model may have higher rise velocities than the prototype, whereas scaled flow velocities are lower in the model. This suggests that the model cannot be operated on Froude law alone to obtain any meaningful results on air entrainment and on air being drawn into the suction pipes.

C. Entrainment of Bubbles into Suction Pipes

As discussed in the above sections, the same bubble rise velocities and relative air concentrations could be expected in the model due to jet impingement, provided the jet impingement velocity in the model is the same as that in the prototype and all the linear jet dimensions are modeled to the geometric scale. The question of how to scale the model flows through the suction pipes (which also governs approach velocities) must also be addressed.

Referring to Figure 6, let us consider a bubble at a location x_p ft from the sump entrance and y_p ft below water surface in the prototype. Let $(u_b)_p$ be the bubble rise velocity and let $(u_a)_p$ be the approach velocity to the sump. The downward velocity of water in the sump for maximum flow operating conditions could be as high as 0.75 fps, which is much higher than the rise velocities of most of the small size bubbles (less than 1 cm). Hence, it is reasonable to assume that any small bubble that could reach the sump will be carried down the sump to the downstream side of the wall, with a reasonably good chance of being drawn to the suction pipes. The requirement for a bubble to reach the sump is

$$\frac{y_p}{(u_b)_p} \leq \frac{x_p}{(u_a)_p} \tag{11}$$

Similarly for the model,

$$\frac{y_m}{(u_b)_m} \leq \frac{x_m}{(u_a)_m} \tag{12}$$

If the model produces the same bubble size range as in the prototype and the same air concentrations due to jet impingement, then $(u_b)_m$ will be the same as $(u_b)_p$. If the model jet impingement locations and water depths are fixed to the geometric scale L_r, we get

$$\frac{y_m}{y_p} = \frac{x_m}{x_p} = L_r \tag{13}$$

Based on Equations (11) to (13) for similarity of bubble motion, it is essential to have

$$(u_a)_p = (u_a)_m \tag{14}$$

This means the approach velocities in the model and prototype should be the same. This, by coincidence, is the same as the "equal velocity rule" used in the model tests for investigating vortex severities.

The flow patterns in the sump portion downstream of the crane wall to the suction pipes can be considered similar between the model and prototype, being closed conduit flow at sufficiently high Reynolds numbers.

MODEL DESCRIPTION AND INSTRUMENTATION

General Layout

A physical model of the containment sump and a portion of the reactor building forming the approach to the sump were constructed to a geometric scale of approximately 1:2.5 on an elevated platform, as shown in Photograph 1. Details of the model construction, dimensions, and general piping arrangement are included in an earlier ARL report (1).

Supply Loop for Break and Drain Flows

Figure 7 and Photograph 2 show the arrangement of supply pipes for break and drain flows. A 75 HP high head pump (300 ft) was used to recirculate the water from the model (taking suction from a location behind the flow distributors) through the break and drain flow pipes. The separate supply pipes connected to break and drain locations, each contained a calibrated orifice meter and a bypass line for flow measurement and adjustment.

The supply pipe for break flow ended in a flexible hose which, in turn, was attached to a nozzle or a circumferential pipe ring (depending upon the type of break to be modeled) at the desired location. The pipe ring was essentially a circumferential ring of 2 inch diameter pipe fastened around the break pipe at the appropriate location and was provided with

slots 1/8 inch wide and 1 inch long and at about 1 inch spacing for half the circumference at a desired angle, as shown in Photograph 3. The open area of the slots was kept as the scaled area from the assumed prototype break area. Only half the circumference was provided with slots to make the flow directed towards the sump, as a conservative assumption. The ring was set so as to make the slots facing the sump and the slots were cut at about 60° to the horizontal so as to direct the flow right at the sump entrance onto the water surface. This simulated rectangular jets from circumferential breaks. A nozzle of suitable diameter (giving the same flow area at the break) was used when a circular jet was simulated.

The supply pipe for drain flow ended at the modeled drain locations, with a flexible hose incorporated such that the pipe end could be directed at a desired location. The pipe sizes scaled the prototype drain diameters.

Modeling of Break Flows

Break flow locations 1 and 2 (Figure 3) were modeled as a single location, as were 4 and 5, as these two locations are very close to each other. Cross-over break locations 3 and 8, location 9 in the hot leg, and locations 6 and 7 in the 3 inch and 2 inch pipes, respectively, were modeled separately. The area of the circumferential breaks in the model was scaled from the given (assumed) prototype area of 25 square inches. A rectangular jet formed by slots described earlier along half the circumference of the pipe facing the sump was modeled and tested at all locations in the cross-over loop and hot leg. The 3 inch and 2 inch pipe breaks were modeled only as circular jets similar to those possible in the prototype. Photograph 4 shows the slotted circumferential pipe at location 2 and the break flow issuing out of it directed at the sump.

The jet velocity of impact at the water surface was calculated for the prototype breaks using the break flow and area and height of fall as,

$$u_j = u_{je} + \sqrt{2g\ H} \qquad (15)$$

where u_{je} is the exit velocity given by Q_b/A_b, the ratio of break flow to area and H is the height of fall. The model break flow required to give the same value of u_j was then calculated as the break area and height of fall in the model are known. This value was set in the model.

Modeling of Drain Flows

Ice condenser drain flow locations 1 and 2 (Figure 4) were modeled being very close to the sump. Locations 3 and 4 were considered unimportant as the drain flow jet at location 3 would mostly be intercepted by the steam generator and its supports and the jet at location 4 was considered too farther away from the sump. In modeling the drain flows, it was considered important to simulate the drain pipe diameter and height of the drain to the geometric scale. The point of impingement of the drain flow jet on water surface was located for the Froude scaled flow through the drain, as the path of drain flow essentially was gravity controlled. Once this impact point was located, the flow was increased to give prototype impingement velocity, at the same time adjusting the flexible hose end of the model drain suitably to keep the impingement region the same. The prototype velocity of impingement was calculated using Equation (15).

TEST PROCEDURE

Tests to investigate air-entrainment in the sump area due to the impingement of high velocity break and drain flows on the water surface were considered necessary for break locations or drain locations close to the sump so that impingement could take place in the immediate vicinity of the sump. It was realized that air could be drawn into the suction pipes either directly from the impinging jet or after a sufficient quantity of small bubbles collected on the top cover of the sump. The objectionable limit of air entrainment was considered to depend on the pump, and this limit was not known. In general, any air entrainment of large bubbles into the suction pipes was deemed objectionable.

As discussed in earlier sections of the report, since bubble sizes and bubble rise velocities do not scale in a Froude model, special test procedures were used to approximate the prototype conditions. The test procedure followed is described below.

a. The breakflow or drainflow areas and their locations were modeled based on the geometric scale of the model. Breakflow types, whether circumferential or circular, were used in deciding the jet dimensions to give the proper scaled area.

b. Only one break was considered possible at a time. A worst possible direction of the jet towards the sump entrance was assumed. For drain flow jets, an impact point was determined by scaling the correct water level and Froude scaled flow for each location of drainflow.

c. The jet flow was increased to give prototype impact velocities of the jet, and the jet direction was adjusted to keep the same impact location decided from step b. To accomplish the reorientation, adjustable connections to the break nozzles (or slotted ring) or drain pipe ends were provided.

d. The model was run so that prototype velocities were obtained in the pump suction pipes corresponding to possible prototype flow combination. The submergences (or depth of water in the model) corresponded to geometrically scaled values.

e. Air-entrainment in the sump area and in the pump suction pipes was ascertained by observing any air collected on the top covers of the sump or being drawn into pipes. Photographic documentation as required was obtained.

f. If objectionable conditions were noted, modifications such as adding baffle plates, deflectors, air vents, etc., were implemented. Major sump location or configuration changes were considered only if absolutely essential.

g. The above steps were repeated for each water level and flow condition and for each break or drain flow locations. Also, the effects of screen blockages (up to 50%), using the same worst blockage schemes derived from vortexing tests, were investigated.

h. While performing the tests, any increased vortex activity due to modifications were observed. If objectionable air-pulling vortices were present, alternative modifications were tried.

Modeling of Air-Venting System at Top Covers

The earlier ARL study (1) on the vortexing behavior of the sump had indicated the necessity of improving the air-venting at the top covers both upstream and downstream of the crane wall. For the upstream top cover, it was recommended that one row of 1/2 inch diameter holes be provided at about 18 inches c/c, and these holes were modeled to scale.

For the downstream top cover, sloping roof plates angled up towards a single vent pipe was proposed by AEPSC, as shown in Figure 8. This venting system was built to scale in the model. The horizontal slab above the sloping plates was not modeled, being unnecessary.

RESULTS

Air-Entrainment due to Drain Flow

Drain flow at the modeled locations could exist for a case when the recirculation mode is initiated at EL 602 ft 10 inches (operating case 1a or 1b only) whereas the break flow at the locations in the cross-over leg in the vicinity of the sump model have to be considered only for a case when the recirculation mode is initiated at EL 607 ft 4 inches. Hence, drain flow jet impact tests were conducted first for one pipe operation cases (1a and 1b of Table 2). In this case, the sump entrance was not

submerged, the top cover being at EL 604 ft 11-3/8 inches. Considerable air-entrainment was generated at the impact location as seen in Photograph 5. Most of the bubbles, being large (of sizes greater than 5 mm), were not drawn down into the sump under the crane wall. However, small quantities of relatively smaller bubbles were pulled down the upstream sump portion into the downstream area, and most of these collected at the top cover in the downstream portion. The air-vent system of single vent pipe and sloping plates (Figure 8) was not efficient enough to vent all the bubbles collected. This caused accumulation of bubbles and occasional pulling of slugs of air into the suction pipe (more so with a 50% blockage of sump screens).

It was decided to extend the drain flow pipes farther from the sump area, along the crane wall, to allow them to discharge at a submerged location away from the sump entrance area, thereby totally eliminating the drain flow jet impact in front of the sump. With this change, further testing was carried out without drain flow modeling.

Air-Entrainment due to Break Flows

A. Unsubmerged Break Locations

A high velocity jet impact at the water surface occurred for modeled break locations 1 (or 2) and 4 (or 5) (Figure 3), which were not submerged for the lowest water elevation of EL 607 ft 4 inches, at which operating case 1a or b was possible. These break locations were tested one at a time. Even though they produced considerable air entrainment, no air bubbles of readily visible sizes were seen to be drawn into the sump down the crane wall. This is because the sump entrance was completely submerged with its top cover below the water surface (about 1 ft in model or 2.5 ft in prototype) and most of the air-entrainment was in the top few inches. Photographs 6 and 7 show the air entrainment at the surface in the sump area for break locations 1 and 4. The surface air entrainment, although considerably, was restricted to a small depth and no air bubbles of any

significant size were drawn deep into the sump. No visible quantity of bubbles were drawn into the pipes, as indicated by observations through windows in the pipe. Hence, the sump performance was considered satisfactory with regard to air entrainment due to unsubmerged break jets.

B. Submerged Break Locations

Even though submerged break locations are not likely to produce air-entrainment, particular breakflow orientation could augment any borderline vortex activity by adding more to any existing circulation. With this in mind, all the submerged break locations; namely 3, 6, 7, and 8, were tested (Figure 3) for all operating cases. Break locations 6 and 7 were corresponding to breaks in the 3 inch and 2 inch lines joining the cross-over pipe and were considered as vertical upward or downward circular jets. These submerged vertical jets did not produce any significant vortex activity nor did they cause any air entrainment problems. A vertical upward jet was observed to emerge out of the water surface, but was broken into a spray by hitting objects and was of no concern. Break flow location 8 was seen to have little influence on vortexing and no problems of concern were noticed.

Break location 3 in the bend portion of the pipe when properly oriented, together with a 50% blockage [blockage schemes 3 and 5 of ARL report on vortexing (1)] did add considerable circulation to an otherwise weak surface dimple, frequently producing a strong vortex with an air core extending a few inches below water (Photograph 8). This vortex was very unstable and unsteady, and moved from a position in the center of the sump entrance to a position close to the break flow jet, which caused a dispersion of the air core to a stream of bubbles directed towards the sump. These bubbles were large enough and had enough buoyancy not to be drawn under the crane wall into the downstream portion of the sump. This type of vortex occurred for both operating cases 1 and 2 (water levels 607 ft 4 inches to 610 ft 0 inches).

Sump Modifications and Retesting

The vortexing described in the earlier paragraph was outside the sump, and the sump screens and gratings presumably acted as vortex suppressors as no vortex core was seen extending into the sump. If it is desired to reduce this vortexing, a possible method would be to install a vertical standard floor grating, in front of the horizontal cross over pipe, extending over a length and height to obstruct the break flow jets from locations 3 or 8, as shown in Figure 9. It was observed in the model that a grating of 1 inch deep bearing bars served to disperse the jet so as to reduce its contribution to rotational flow field.

The addition of the grating showed a decrease in vortex strength and frequency at the lower water level for the one pipe operation (Photograph 9a). Infrequently, a weak surface dimple vortex moved towards the break flow jet which dispersed few large bubbles towards the sump, however, none of these bubbles entered the downstream sump region. For both pipes operating at a water level of EL 610 ft, the vortex intensity was reduced by the extra grating to a surface swirl and no significant activity was present (Photograph 9b).

Air Venting at Downstream Top Cover

In general, the right side of the sump roof downstream of the crane wall was found less efficient in air-venting compared to the left side, where the single air-vent pipe is located. Since no objectionable rate of air accumulation and withdrawal through the suction pipes were noted for any of the test conditions, there appears little need for any modification or redesign of the top cover. However, some additional efforts were made to evolve a design to improve the air-venting, in case it is desired.

The sloping plates attached to the original horizontal slab bottom were modeled along with the vent pipe (Figure 8). However, the horizontal slab itself was not included in the model, being unnecessary for simulating the air venting system, which essentially consisted of the sloping plates and vent pipe. To improve the performance of this vent sys-

tem, it was decided to provide a few 1/2 inch diameter holes at 5 inches c/c in the model along the portions of sloping cover plate on the right side of the sump away from the main vent pipe. As the horizontal slab was not modeled, the holes were all connected to a common manifold located approximately at the same elevation corresponding to the bottom of the horizontal slab above the plate. The common manifold, in turn, was connected to an additional vertical vent pipe. Such an arrangement was seen to improve the venting system, reducing the accumulation of bubbles under the sloping plate. The bubbles continuously escaped through the holes and were eventually flushed through the additional vent pipe.

CONCLUSIONS

1. Drain flow jets impinging in front of the sump produced considerable air-entrainment. For lower water levels (at or about EL 602 ft 10 inches), the sump entrance was not submerged (free surface present inside sump) and small quantities of smaller size air bubbles were drawn with the flow to the portion of the sump downstream of the crane wall. In spite of the air-venting system, some of the bubbles were collected under the top cover and were occasionally drawn into the suction pipe. To avoid this, it is recommended to redirect the drain flow at locations 1 and 2 (Figure 4) away from the sump area by extending the drain pipes along the crane wall and preferably discharging the drain flow close to or beneath the water surface in the sump.

2. Break locations 1, 2, 4, 5, and 9 (Figure 3) could cause unsubmerged high velocity jets impinging on the water surface near the sump entrance for a range of water levels below the corresponding break locations. The sump roof and entrance would be submerged for all the possible operating conditions, the sump top cover being below the minimum water level of EL 607 ft 4 inches. The model test results indicated that the unsubmerged jets caused considerable air-entrainment at and near the impact region. However, no noticeable movement of bubbles to the sump portion

downstream of the crane wall was observed for the above break locations. This could be due to sufficiently high water depths and low approach velocities, which allow bubble release to surface, and also due to the fact that the sump entrance was well submerged (more than 2 ft) below the water surface. Hence, no adverse air-entrainment problems were encountered for unsubmerged breakflow jets.

3. No submerged break flow tested caused any air-entrainment. However, it was important to assess the probable contributions of submerged break flows in augmenting vortexing to any objectionable extent, as noted below.

   a. Break locations 6 and 7 generated vertical circular jets in the corresponding 2 inch or 3 inch pipe. These jets were submerged for all operating conditions, and were seen to cause no vortexing problems even with 50% screen blockages.

   b. Break locations 4 and 5 (circumferential breaks) were submerged for water levels higher than their locations. At these water levels, model tests indicated no significant vortexing problems, even with 50% screen blockages.

   c. Break locations 3 and 8 were submerged for all operating conditions. n Breakflow at location 8 did not cause any objectionable vortexing problems. However, break flow at location 3 was observed to strengthen a weak dye-core type vortex which existed even without breakflows (see ref. 1) outside the sump screen between the vertical legs of the cross-over line. This vortex was unstable and intermittent and was seen to have an air core extending to a few inches below the water surface when tested with 50% screen blockage. When such an air core formed, and the vortex moved towards the break, the

breakflow jet was seen to break the core into bubbles. Some of these bubbles entered the sump area, but were large enough to escape to the surface and were not drawn to the portion of the sump downstream of the crane wall (and hence not drawn into suction pipes). As an option, this vortex severity could be reduced considerably by placing a standard floor grating (2-1/2 inch deep bars) as indicated in Figure 9.

4. There appears little need for any redesign or modifications of the sump top covers, as no objectionable rate of bubble accumulation underneath these covers were noted for the test conditions with the drain flows redirected. The rate of air venting in the downstream sloping top cover plate could be further improved if an additional vent pipe were to be provided in the right portion of the sump cover (looking downstream) and a few rows of 1-1/4 inch diameter holes at about 12 inches c/c are drilled on this portion of the plate.

REFERENCES

1. Padmanabhan, M., "Hydraulic Model Investigation of Vortexing and Swirl Within a Reactor Containment Recirculation Sump - Donald C. Cook Nuclear Power Staton," ARL Report No. 108-78/M178PF, September 1978.

2. Murakami, M., et al., "Flow of Entrained Air in Centrifugal Pumps," 13th IAHR Congress, Japan, August 31 to September 5, 1969, Vol. 2, p. 71- 0.

3. Rouse, H., Handbook of Hydraulics, John Wiley & Sons, 1950.

4. Anwar, H.O., "Prevention of Vortices at Intakes," Water Power, October 1968, p. 393.

5. Ervine, D.A., and Elsawy, E.M., "The Effect of a Falling Nappe on River Aeration," IAHR 16th Congress, San Paulo, Brazil, 1975, Vol. 3, p. 390-397.

6. Elsawy, E.M., and McKeogh, E.J., "Study of Self-Aerated Flow with Regard to Modeling Criteria," IAHR 17th Congress, 1977, Vol. 1, p. 475-482.

7. Govier, G.W., and Aziz, K., Flow of Complex Mixtures in Pipes, Van Nostrand Reinhold, 1972.

8. Chanishvilli, A.G., "Air Entrainment and Vertical Downward Motion of Aerated Flows," IAHR 8th Congress, Montreal, Canada, 1959.

TABLES

TABLE 1

Break Flows*

1. Break locations in the cross-over and hot legs (circumferential breaks)

   Break Area = 25 sq. inches.

   Maximum flow of 540 lb/sec occurring at 15 minutes after LOCA.

2. Break location in 3 inch Sch. 160 line.

Time from LOCA, secs	Mass Flowrate (lb/sec)
750	116.3
1000	114.0
1250	111.3
1500	109.0
1750	108.5
2000	106.0
2500	105.0
3000	100.0

3. Break location in 2 inch Sch. 160 line.

Time from LOCA, secs	Mass Flowrate (lb/sec)
2000	44
3000	42
4000	36.5
5000	33.75
6000	32.25
7000	31
8000	30
9000	28.75

*Details supplied by AEPSC.

TABLE 2

Operating Cases Tested

Operating Case No.	Flow/Pipe gpm	Range of Water Surface Elevation	Remarks
1a	9500	602'10" - 606'0" 607'4" - 610'0"*	Runout condition of one ECCS train upon complete failure of other. Left pipe operational.
1b	9500	602'10" - 606'0" 607'4" - 610'0"*	Runout condition of one ECCS train upon complete failure of other. Right pipe operational.
2	7700	606'0" - 612'0" 610'0" - 612'0"*	Runout condition of ECCS pumps with both trains operating.
3a	1 x 9500 1 x 3600	606'0" - 612'0" 610'0" - 612'0"*	Runout condition of one ECCS train (left); containment spray pump from other train at runout flow (right).
3b	1 x 3600 1 x 9500	606'0" - 612'0" 610'0" - 612'0"	Runout condition of one ECCS train (right); containment spray pump from other train at runout flow (left).

*Applicable for break flow tests.

PHOTOGRAPHS

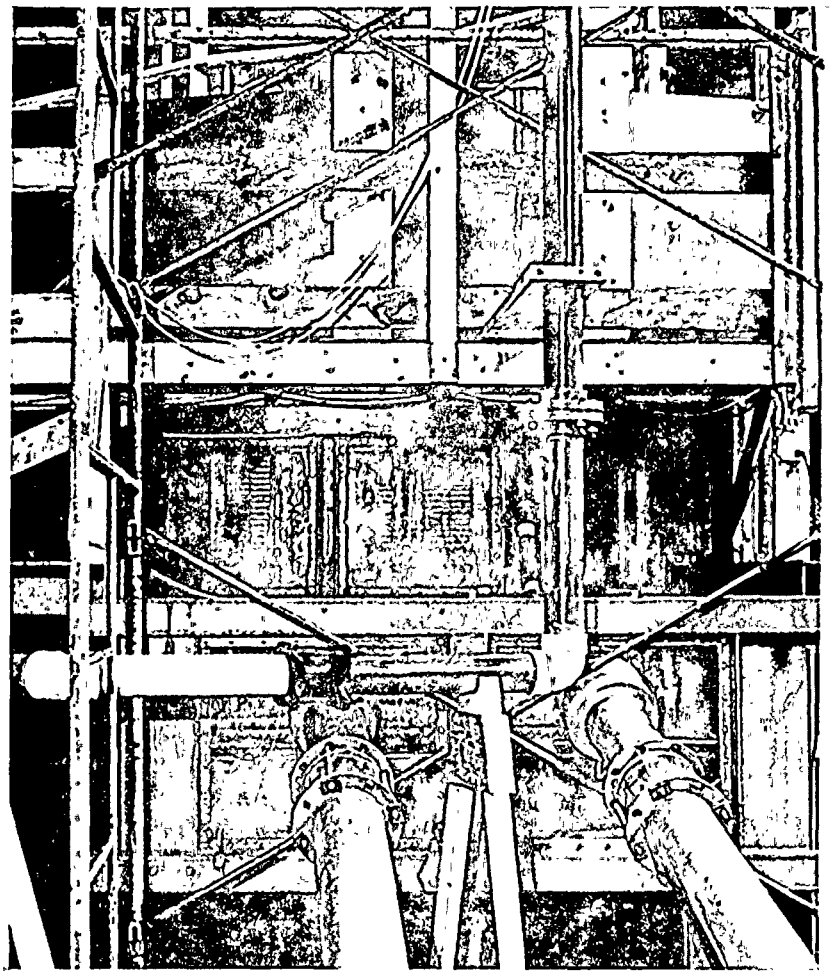

Photograph 1 Overall View of Sump Model (1:2.5 Scale)

Photograph 2 Model Simulation of Break and Drain Flows

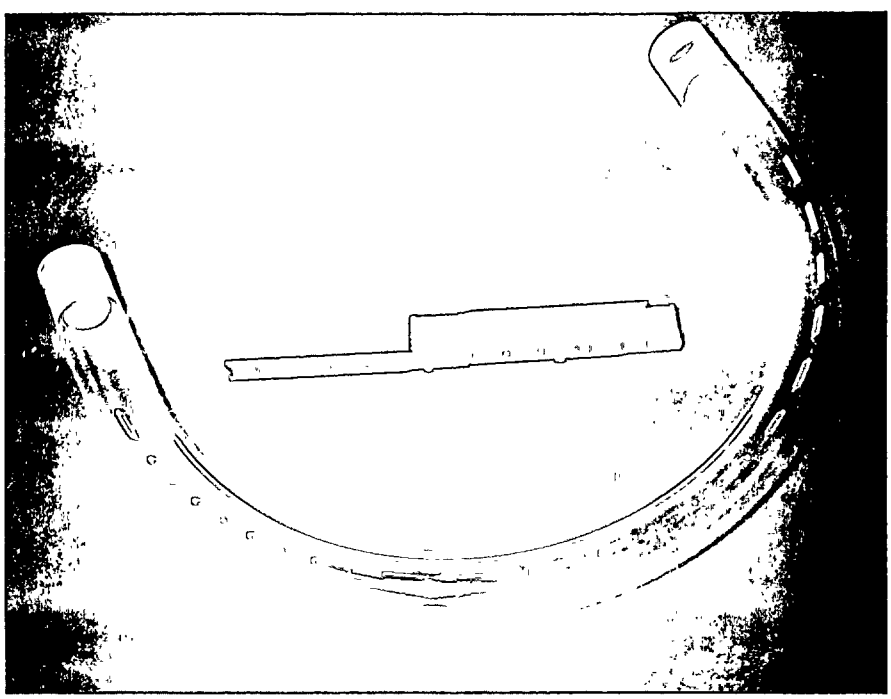

Photograph 3 Simulation of Circumferential Break Area

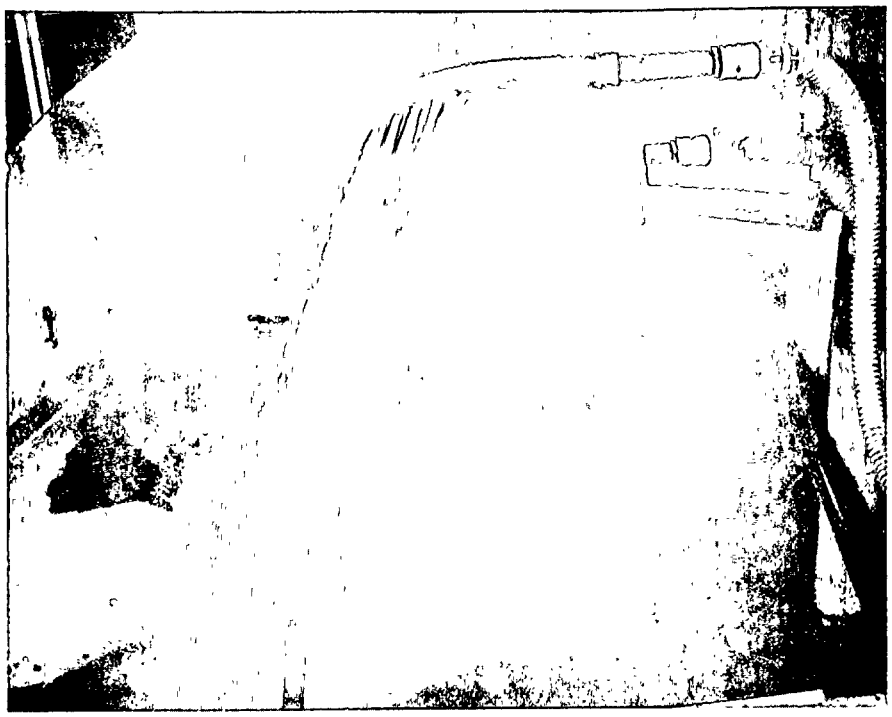

Photograph 4 Typical Circumferential Break Flow

Photograph 5 Drain Flow Impingement; Water Level EL 602'10"

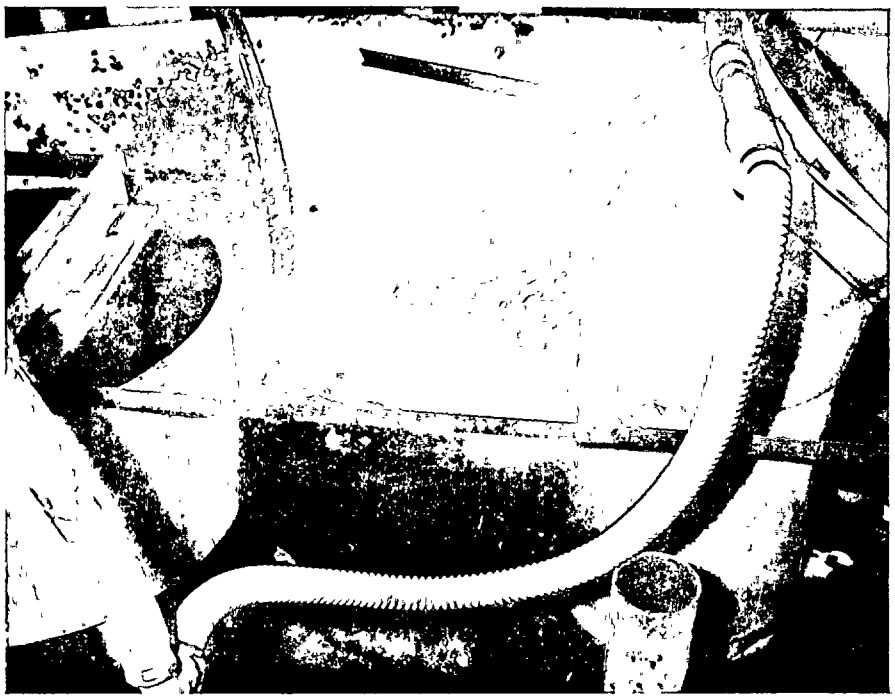

Photograph 6 Break Flow Impingement; Break Location 1; Water Level EL 607'4"; Operating Case 1

Photograph 7 Break Flow Impingement; Break Location 4; Water Level EL 607'4"; Operating Case 1

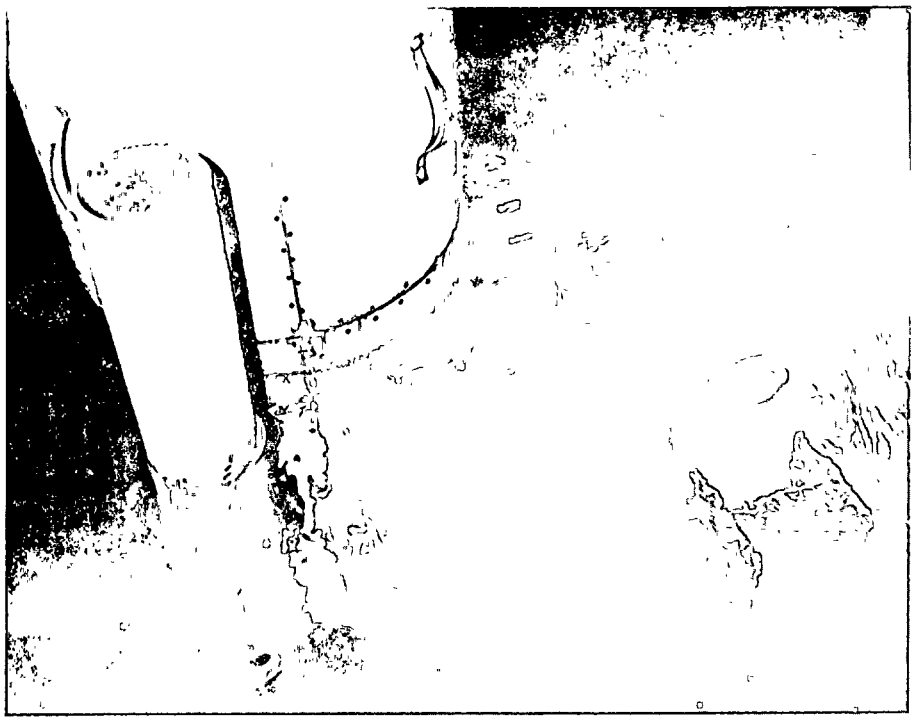

Photograph 8a Submerged Break Flow; Break Location 3; Water Level EL 607'4"; Operating Case 1

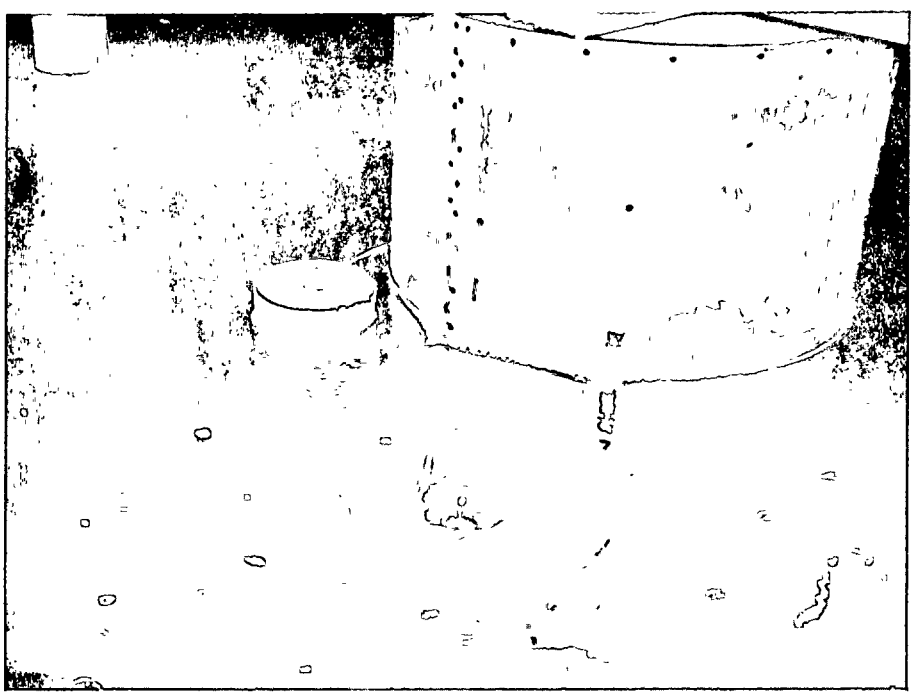

Photograph 8b Submerged Break Flow; Break Location 3; Water Level EL 610'0"; Operating Case 2

Photograph 9a Submerged Break Flow; Break Location 3; Water Level EL 607'4"; Operating Case 1; With Vertical Grating for Jet Interception

Photograph 9b Submerged Break Flow; Break Location 3; Water Level EL 610'0"; Operating Case 2; With Vertical Grating for Jet Interception

FIGURES

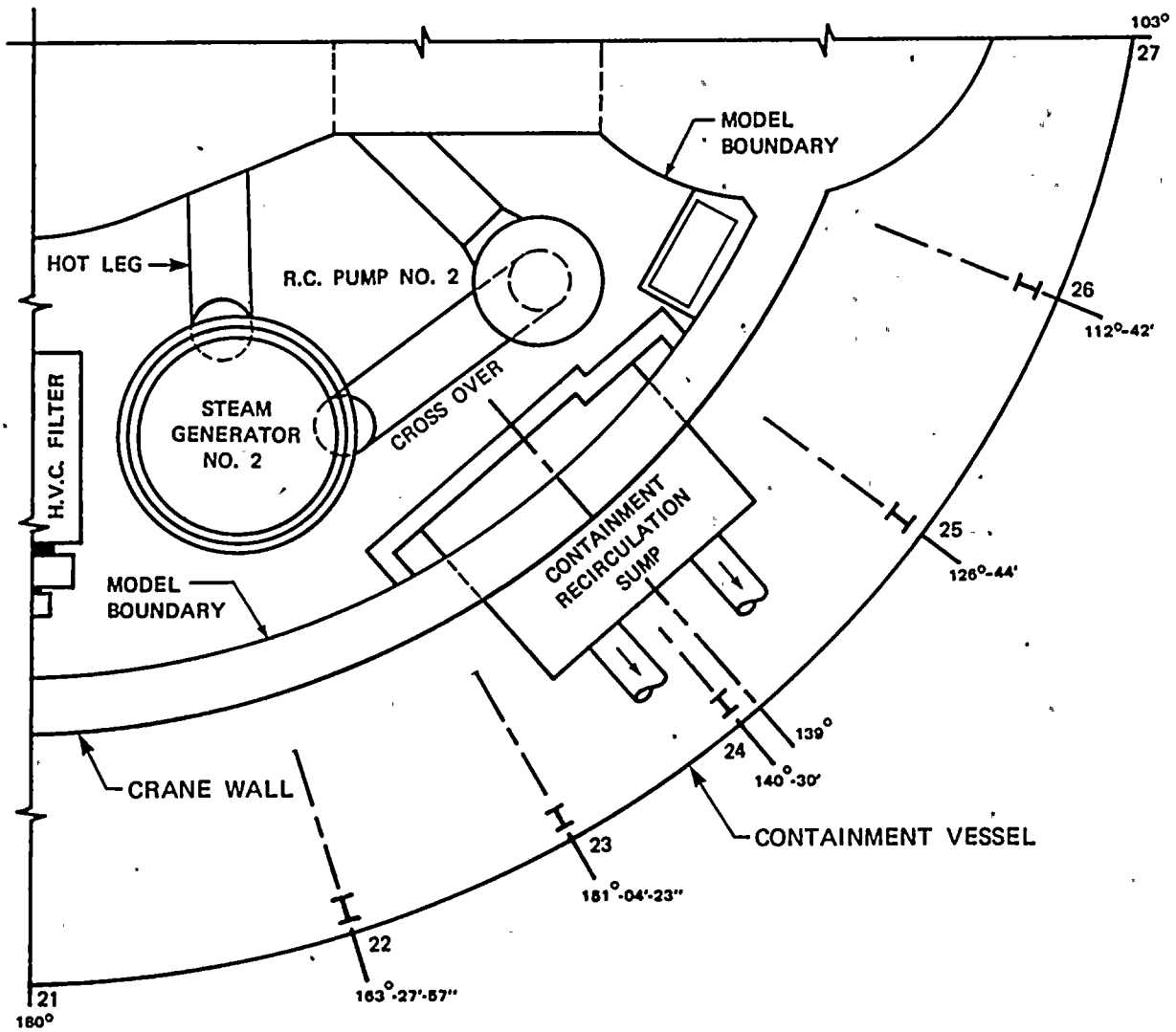

FIGURE 1 LOCATION OF SUMP WITHIN CONTAINMENT BUILDING

ARL

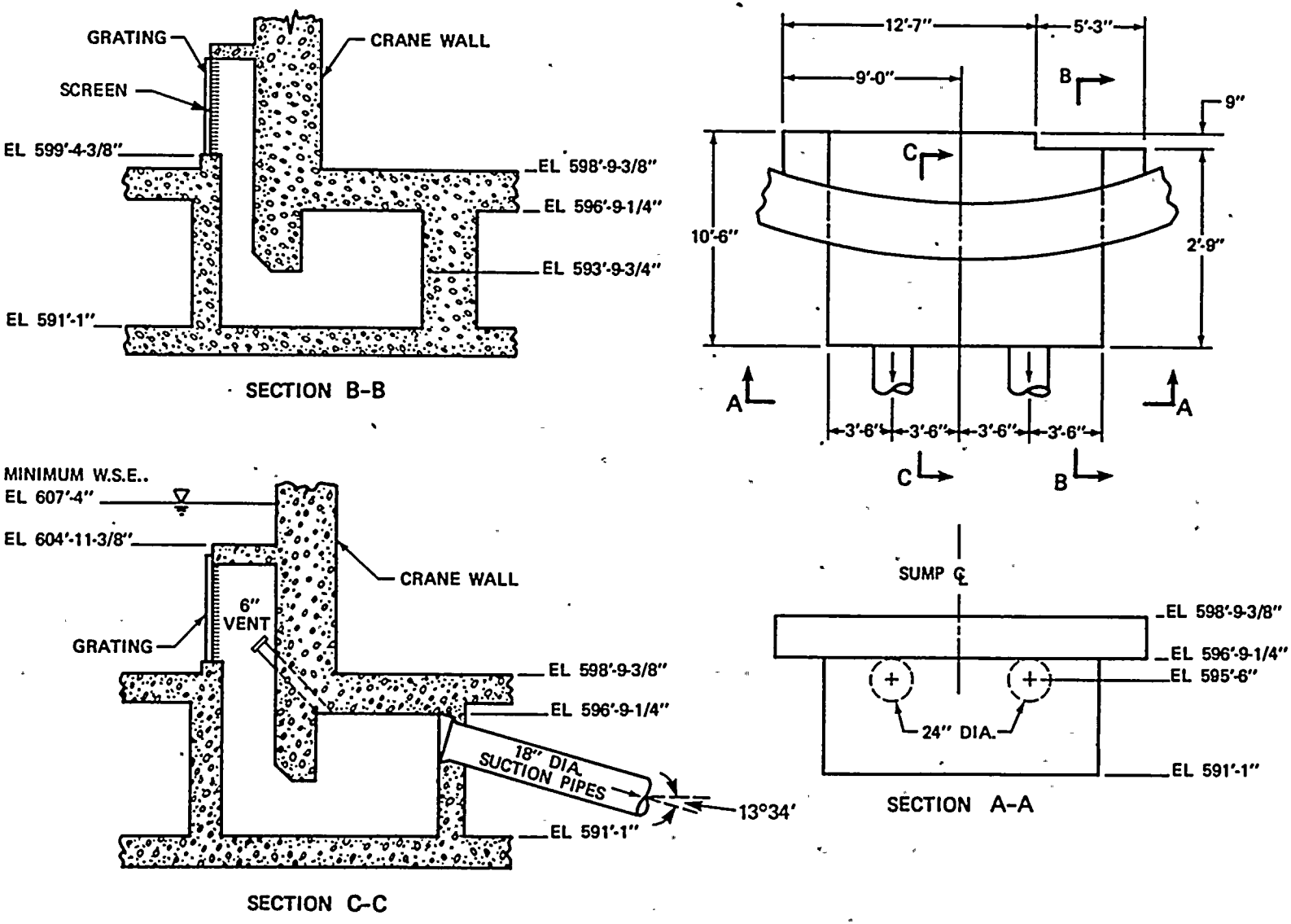

FIGURE 2 DETAILS OF ORIGINAL SUMP

NOTE:

BREAK	ELEVATION
1	615'-11"
2	615'-8-3/4"
3	604'-11-1/2"
4	608'-2-1/4"
5	608'-5"

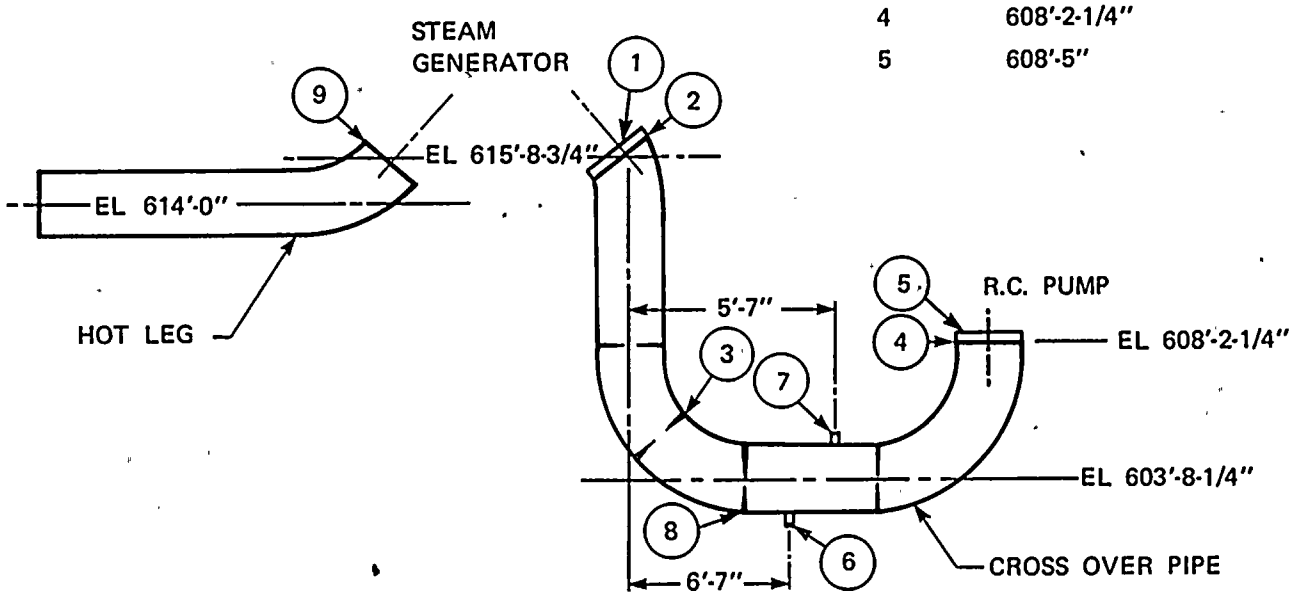

EVENT	WATER LEVEL IN SUMP
SWITCHOVER OF FIRST ECCS TRAIN (BREAK OUTSIDE BIOLOGICAL BOUNDARY)	607'-4"*
SWITCHOVER OF SECOND ECCS TRAIN	610'-0"
WATER LEVEL (CONSIDERING PARTIAL ICE CONDENSER MELTDOWN) AT SWITCHOVER OF SECOND ECCS TRAIN	612'-0"
SWITCHOVER OF FIRST ECCS TRAIN (BREAK INSIDE BIOLOGICAL BOUNDARY)	602'-10"*

*BASED ON NO ICE CONDENSER MELT FROM ICE CONDENSER

FIGURE 3 POSTULATED BREAK LOCATIONS

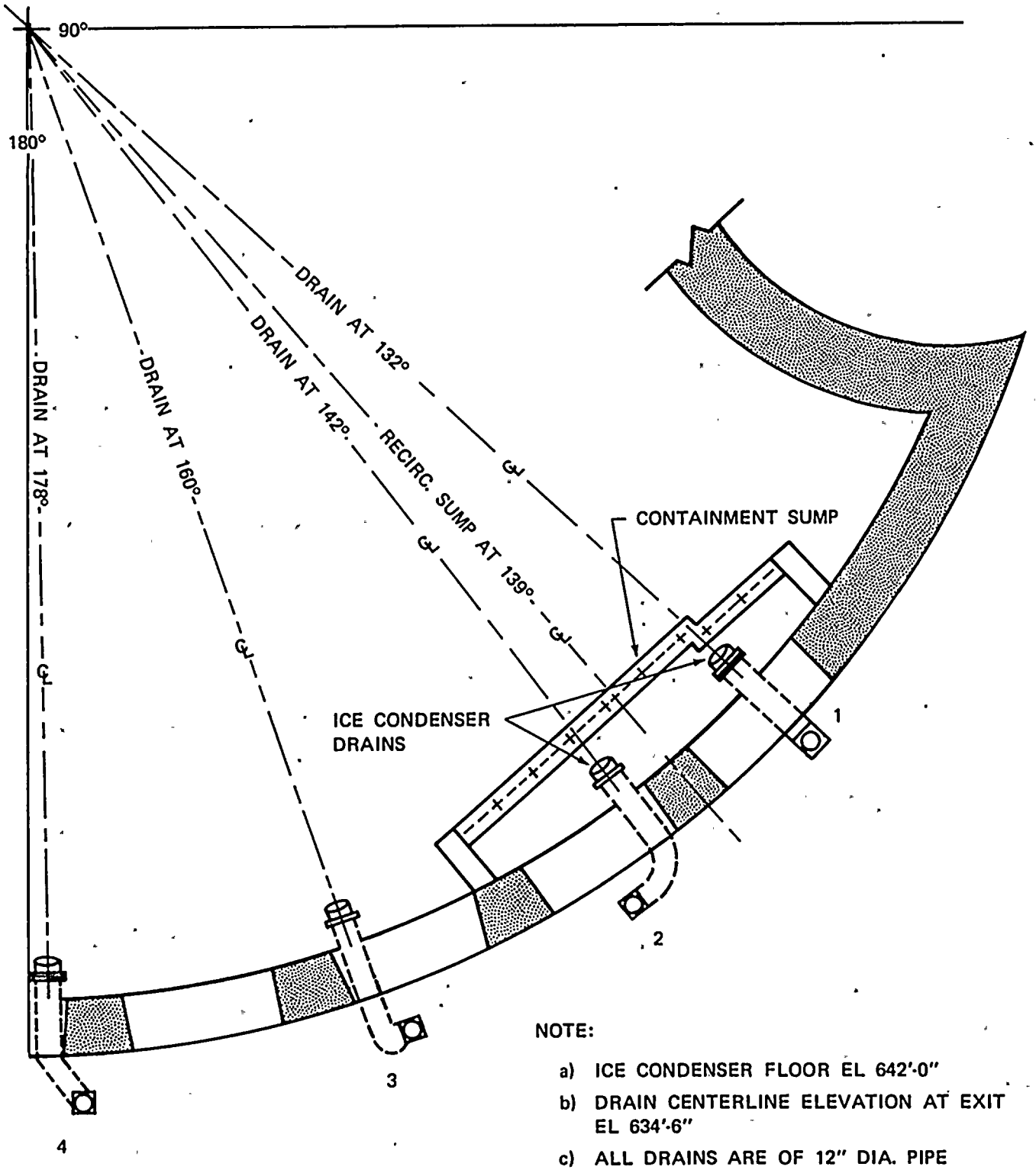

NOTE:

a) ICE CONDENSER FLOOR EL 642'-0"

b) DRAIN CENTERLINE ELEVATION AT EXIT EL 634'-6"

c) ALL DRAINS ARE OF 12" DIA. PIPE

FIGURE 4 DRAIN LOCATIONS

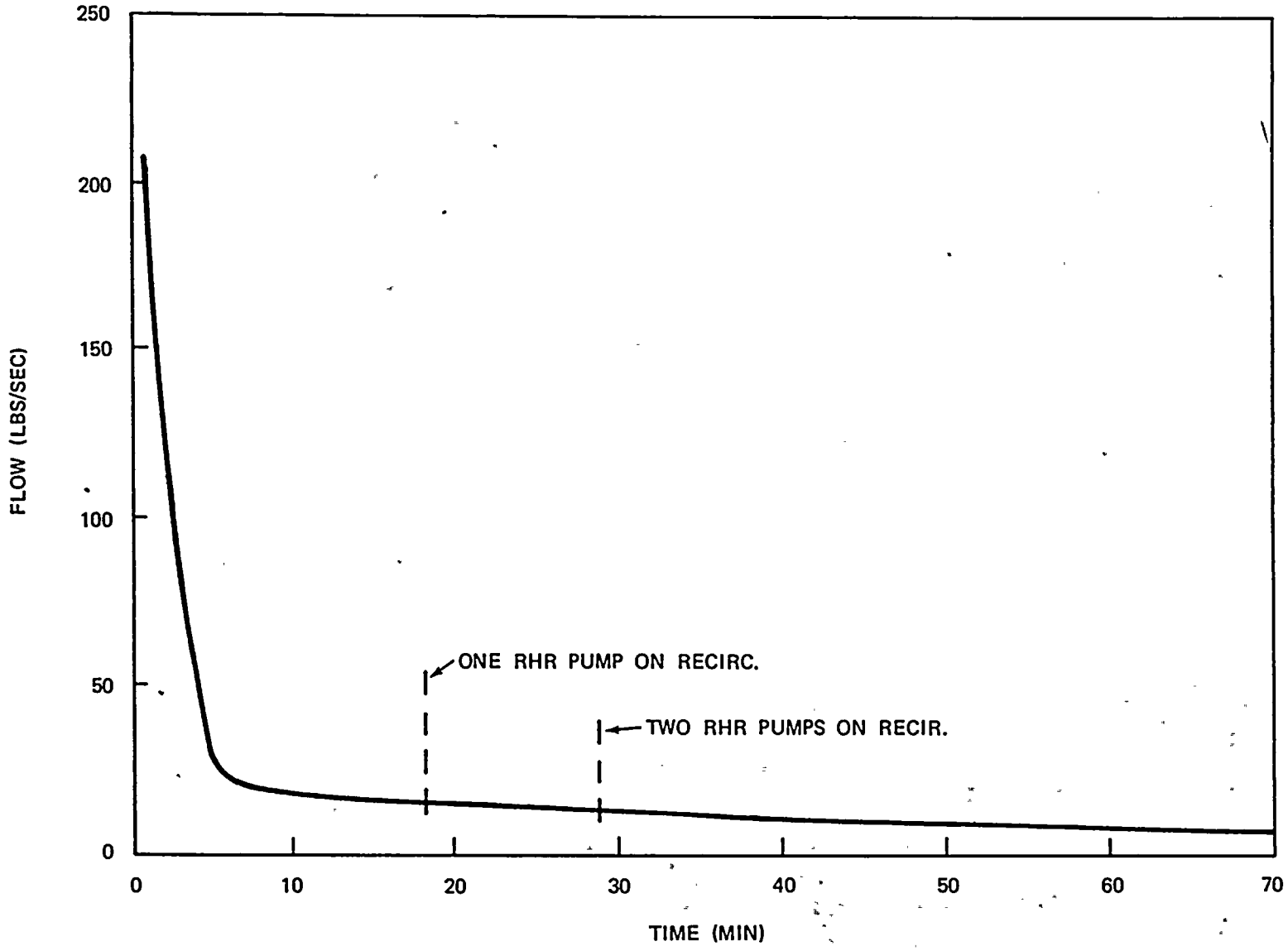

FIGURE 5 POST LOCA FLOWRATE OF EACH ICE CONDENSER FLOOR DRAIN

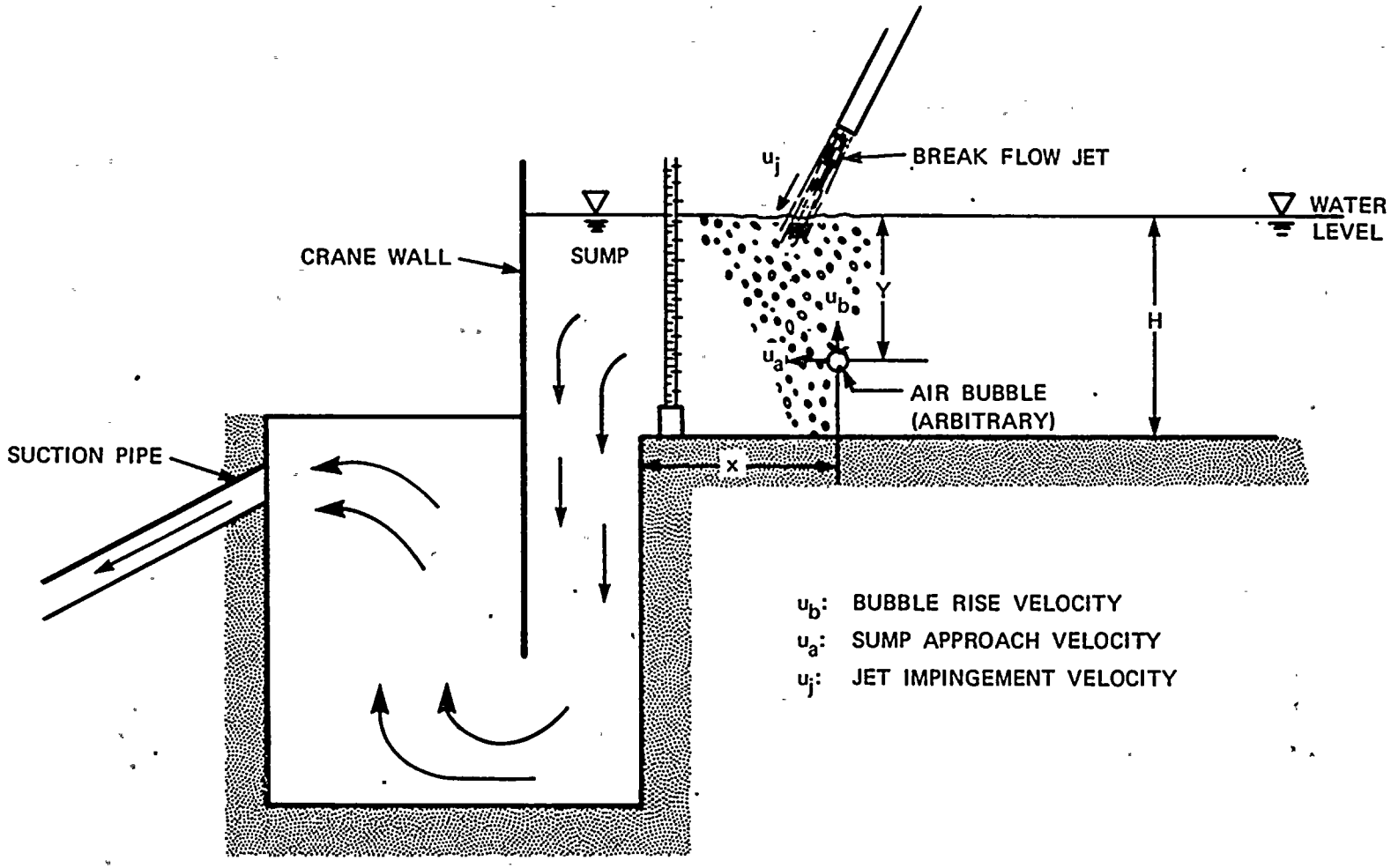

FIGURE 6 DEFINITION SKETCH FOR BUBBLE MOTION TOWARDS SUMP

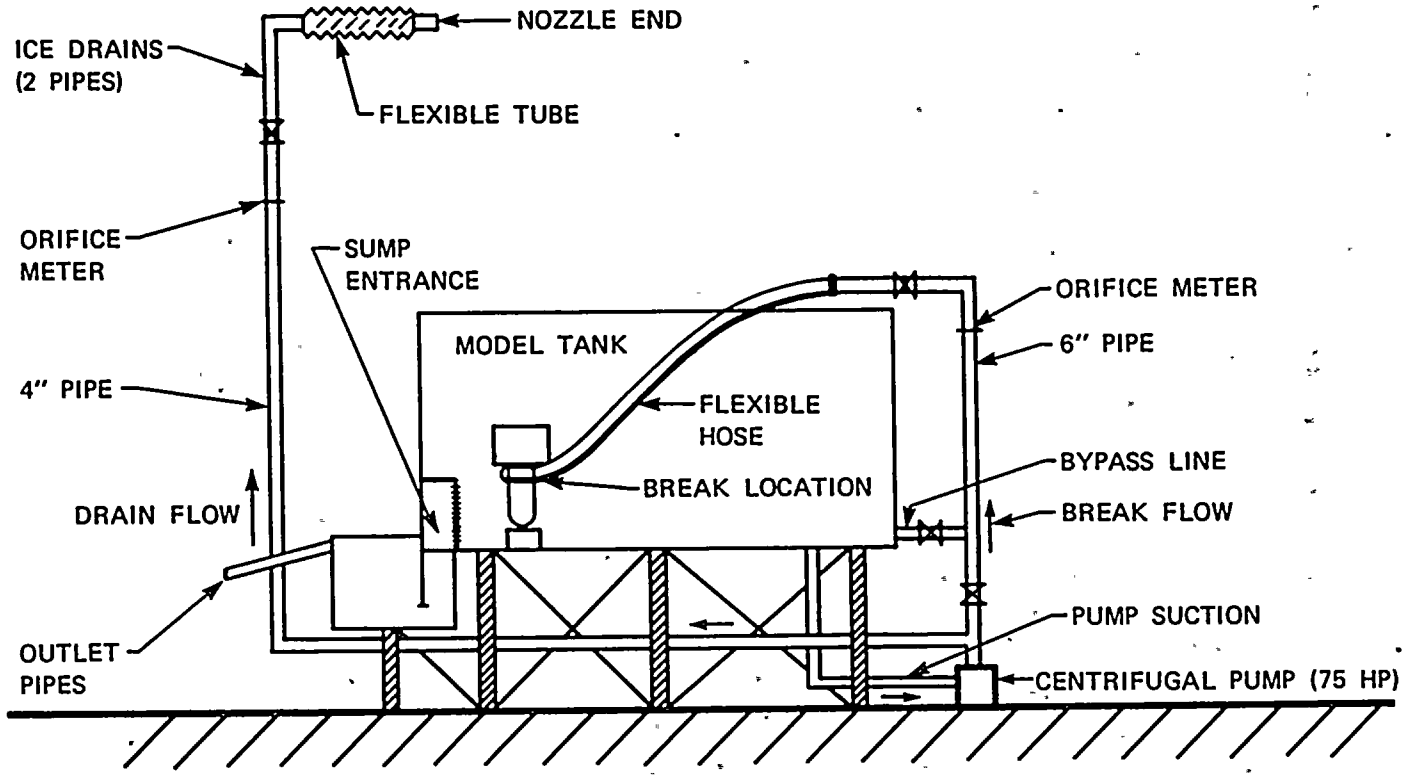

FIGURE 7 SCHEMATIC DIAGRAM OF BREAK AND DRAIN FLOW SUPPLY PIPING IN MODEL

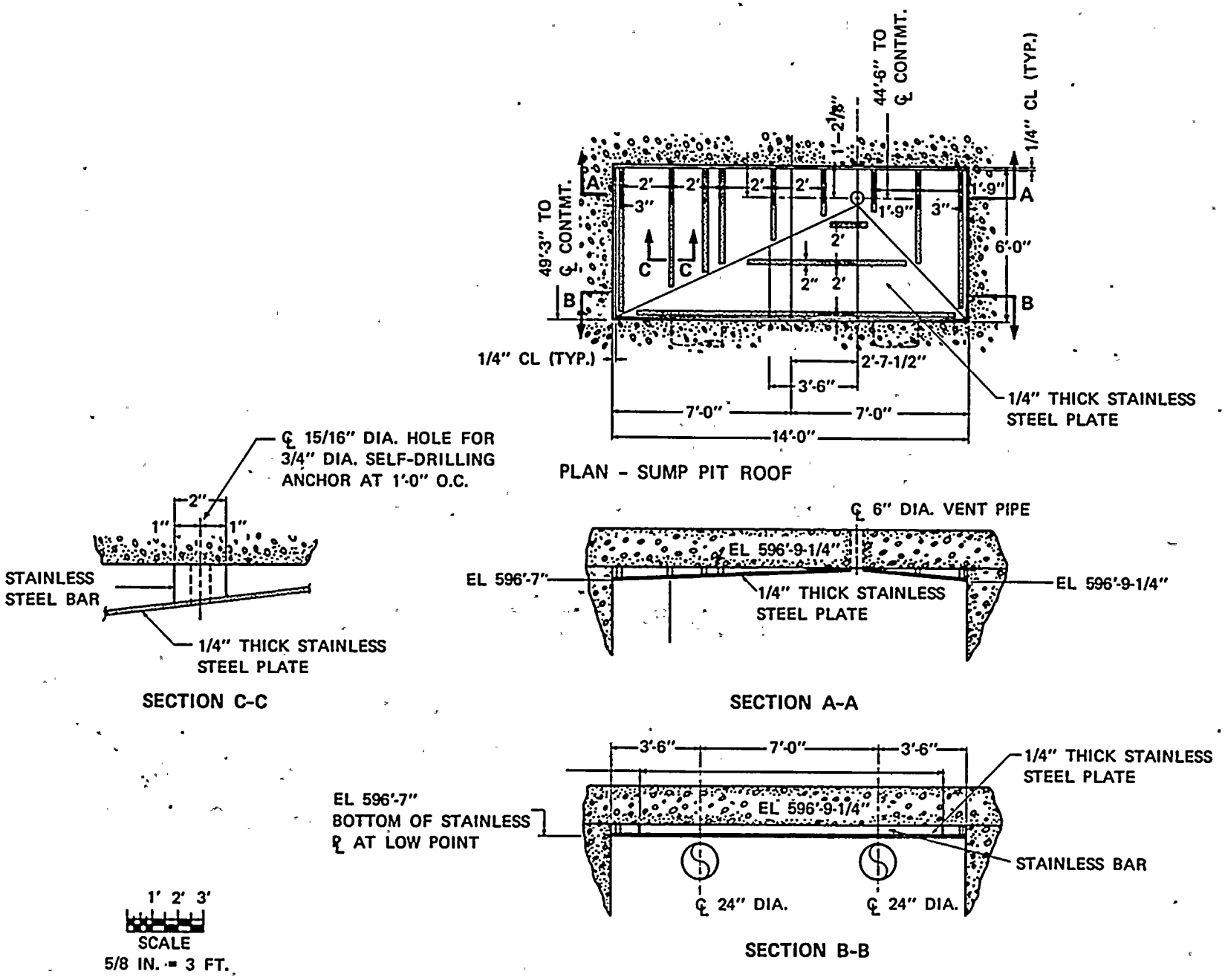

FIGURE 8 IMPROVED AIR VENTING AT TOP COVER

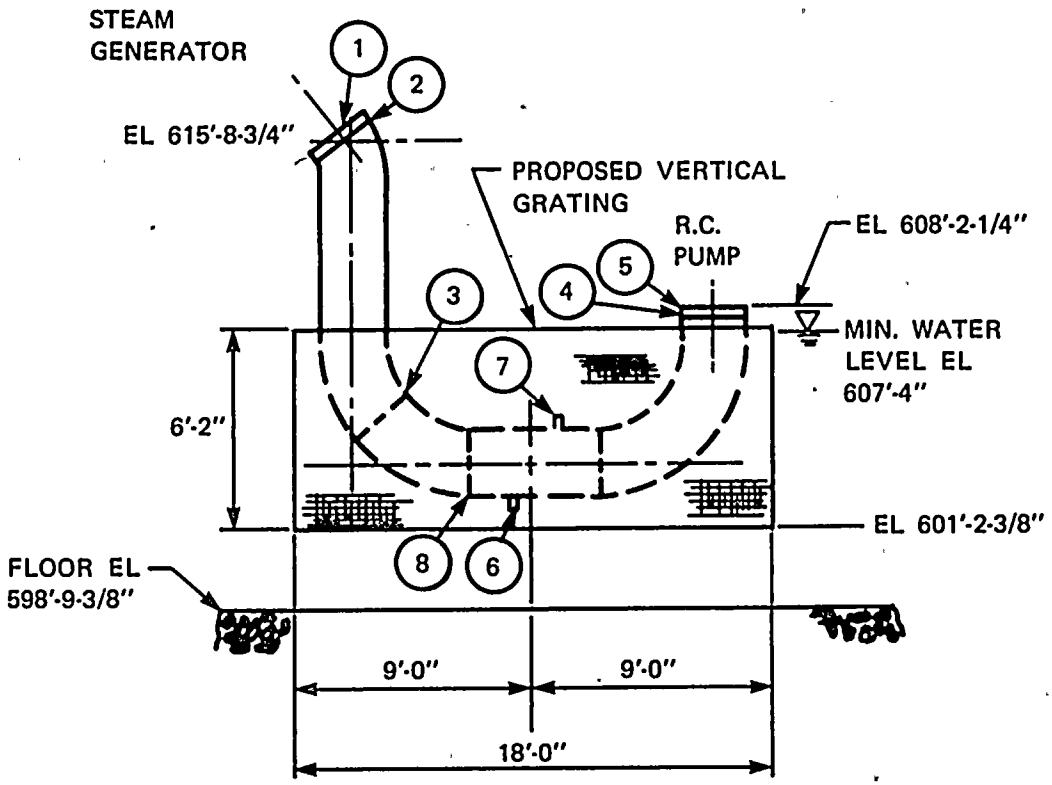

NOTE: 2-1/2" STANDARD FLOOR GRATING TO BE PLACED CLOSE TO THE PIPE.

FIGURE 9 POSITION OF SUGGESTED VERTICAL GRATING (OPTIONAL MODIFICATION)